Micropatterned P(VDF-TrFE) Film-Based Piezoelectric Nanogenerators for Highly Sensitive Self-Powered Pressure Sensors

*Ju-Hyuck Lee, Hong-Joon Yoon, Tae Yun Kim, Manoj Kumar Gupta, Jeong Hwan Lee, Wanchul Seung, Hanjun Ryu, and Sang-Woo Kim**

Here micropatterned poly(vinylidenefluoride-*co*-trifluoroethylene) (P(VDF-TrFE)) films-based piezoelectric nanogenerators (PNGs) with high power-generating performance for highly sensitive self-powered pressure sensors are demonstrated. The microstructured P(VDF-TrFE)-based PNGs reveal nearly five times larger power output compared to a flat film-based PNG. The micropatterning of P(VDF-TrFE) polymer makes itself ultrasensitive in response to mechanical deformation. The application is demonstrated successfully as self-powered pressure sensors in which mechanical energy comes from water droplet and wind. The mechanism of the high performance is intensively discussed and illustrated in terms of strain developed in the flat and micropatterned P(VDF-TrFE) films. The impact derived from the patterning on the output performance is studied in term of effective pressure using COMSOL multiphysics software.

1. Introduction

The emergence of small-scale electronic devices with unprecedented multifunctionalities essentially requires portable, lightweight, and sustainable power sources. Harvesting ambient energy sources including solar, thermal, and mechanical energies from nature has received increasing interest for self-powering electronics and portable devices with low power consumption.[1–4] To harvest mechanical energy wasted in nature, piezoelectric nanogenerators (PNGs) have been intensively developed to harvest mechanical energy with variable amplitude and frequency (such as air flow, raindrop, sound, human motion, and ocean waves).[5–8] To effectively convert various kinds of mechanical energies into electricity for the realization of the fully independent, sustainable, and wireless operation of low power-consuming devices and systems in self-powered mode without any charging of batteries, the development of PNGs with large power-generating performance, high sensitivity, and prominent mechanical durability is extremely important. Up to now, various kinds of PNGs applications have been demonstrated, including self-powered photodetectors, gas sensors, tactile sensors, powering commercial light emitting devices (LEDs), and liquid crystal displays (LCDs).[9–14]

Recently, various types of PNGs made by inorganic semiconducting piezoelectric ZnO nanowires, GaN nanowires, and lead-based and lead-free perovskite materials with large piezoelectric coefficients such as $Pb(Zr,Ti)O_3$ [PZT], $NaNbO_3$, $KNbO_3$, $BaTiO_3$, and $ZnSnO_3$ nanostructures have been successfully fabricated.[15–21] Polyvinylidene difluoride (PVDF) as a piezoelectric polymer has especially attracted much attention in order to fabricate transparent and mechanically durable PNGs with a simple, reliable, and cost effective way.[22,23] It was demonstrated that the poly(vinylidenefluoride-*co*-trifluoroethylene) [P(VDF-TrFE)]-based PNGs could offer multifunctionality such as high sensitivity, flexibility, stretchability, and multishape transformability.[24–29] For stable and continuous self-powered operation of devices and systems, large power output from the PNGs is greatly desirable. In this regard, various types of composite structures such as $NaNbO_3$ nanoparticles/PVDF and multiwall carbon nanotubes/PVDF were utilized to enhance the electric power output from the PVDF-based PNGs and improve the power generation efficiency of PVDF-based PNGs.[30,31] Although the electric power output from the PVDF composite-based PNGs is increased compared to that from the pristine PVDF-based PNGs, the fabrication of PVDF composite-based PNGs still faces challenges such as complex fabrication process, noncost effectiveness, less reproducibility, nonuniform power output, difficulty of interface control between inorganic nanostructures and the PVDF polymer matrix. The development of simple and low cost approach for improving electric power output from PVDF-based PNGs without forming complex composite structures is promising to realize various self-powered device applications.

In this work, we demonstrate a trigonal line-shaped and pyramid-shaped micropatterned P(VDF-TrFE) polymers-based PNGs. The output voltage and current from both

J.-H. Lee, T. Y. Kim, Prof. S.-W. Kim
SKKU Advanced Institute of Nanotechnology (SAINT)
Center for Human Interface Nanotechnology (HINT)
Sungkyunkwan University (SKKU)
Suwon 440-746, Republic of Korea
E-mail: kimsw1@skku.edu
H.-J. Yoon, Dr. M. K. Gupta, J. H. Lee, W. Seung, H. Ryu, Prof. S.-W. Kim
School of Advanced Materials Science and Engineering
Sungkyunkwan University (SKKU)
Suwon 440-746, Republic of Korea

DOI: 10.1002/adfm.201500856

micropatterned PNGs were measured and compared to the output of nonpatterned P(VDF-TrFE)-based PNG under the same vertical compressive force. A photolithography process was used to develop different types of microstructure in P(VDF-TrFE) film. The β phase of micropatterned P(VDF-TrFE) was confirmed by X-ray diffraction (XRD) and Fourier transform infrared (FT-IR) spectroscopy studies. It was found the output voltage and current of microstructured P(VDF-TrFE)-based PNGs showed high value, with nearly five times enhancement in the output voltage and current compared to the flat film-based PNG. COMSOL simulation software was employed to study the power enhancement in term of pressure created under micropatterned and nonpatterned of P(VDF-TrFE) film. In addition, we successfully developed a self-powered pressure sensor and demonstrated that minute pressure deviation caused by water droplet and wind flow on micropatterned PNGs could be detected.

2. Results and Discussion

Schematic illustrations of the flat, trigonal line-shaped, and pyramid-shaped micropattern structured P(VDF-TrFE) layers of the Indium tin oxide (ITO)-coated polyethylene naphthalate (PEN) substrate are shown in **Figure 1**a–c, respectively. To compare the morphology of the flat and patterned P(VDF-TrFE) films, field emission scanning electron microscopy (FE-SEM) images were taken (Figure 1d–f). Cross-sectional FE-SEM images of P(VDF-TrFE) are shown in the inset of Figure 1d–f. The thickness was confirmed to be round 15 µm for all three P(VDF-TrFE) films. The details of the fabrication process of both microstructured and the flat P(VDF-TrFE)-based PNGs are illustrated in Figure S1, Supporting Information. **Figure 2**a presents the XRD spectra of P(VDF-TrFE) film recorded at room temperature. The diffraction peaks at 2θ values of 19.9° were assigned to the reflections of the (110) and (200) orientation planes related to the polar β phase of P(VDF-TrFE). The strong diffraction peak indicated the high degree of crystallinity of the β phase in P(VDF-TrFE). An FT-IR spectroscopy spectrum of the P(VDF-TrFE) thin film (Figure 2b) illustrates three β phase-associated intense bands, with 1288 and 850 cm^{-1} belonging to the CF_2 symmetric stretching with the dipole moments parallel to the polar *b* axis. The 1400 cm^{-1} band was assigned to the CH_2 wagging vibration with the dipole moment along the *c* axis.[28]

We subsequently fabricated flexible PNGs based on the flat and micropatterned P(VDF-TrFE) thin films. The silver (Ag) thin film as a top electrode was deposited on the surface of polymers film. An electric field poling with the same strength was applied on all devices before measuring electric signals. We measured the output voltage and current from the flat and micropatterned P(VDF-TrFE) film-based PNGs by applying a pushing force to the top of the PNGs in the vertical direction using a mechanical force stimulator. Piezoelectric output voltage with an average value of 0.4, 2.0, and 2.9 V and piezoelectric output current with an average value of 100, 500, and 900 nA from the flat, trigonal line-shaped, and pyramid-shaped

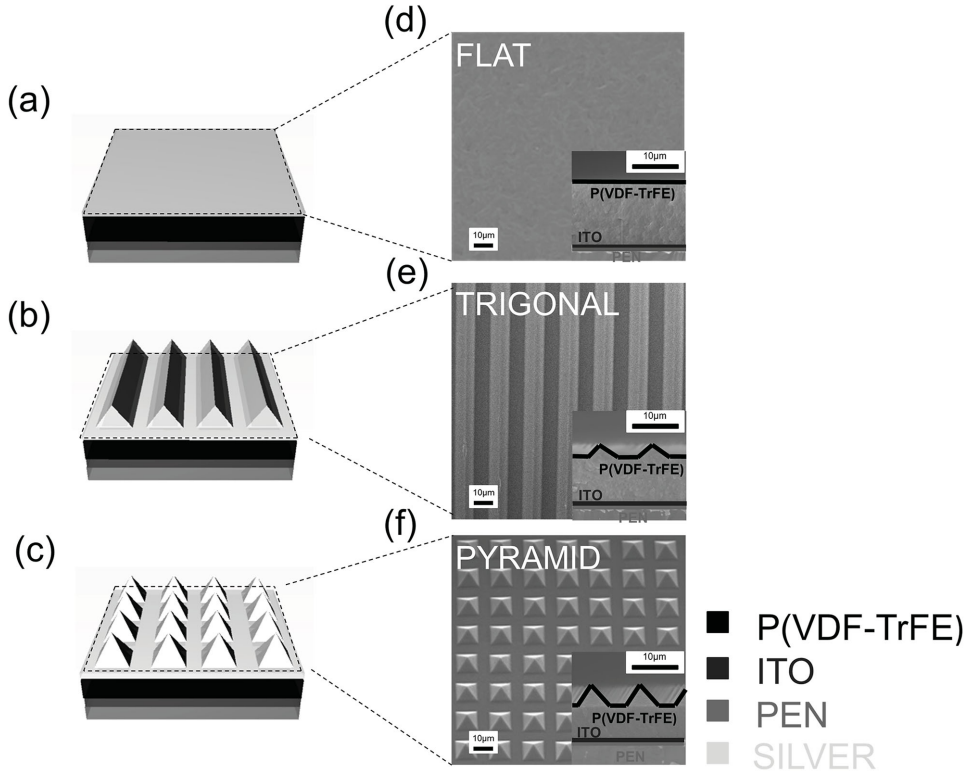

Figure 1. Schematic diagrams of a) flat, b) trigonal line-shaped, and c) pyramid-shaped P(VDF-TrFE)-based PNGs. d–f) Geometrical description through FE-SEM is provided respectively. Insets in FE-SEM images correspond to cross-sectional images of each P(VDF-TrFE)-based NGs (scale bars suggested for each description is 10 µm).

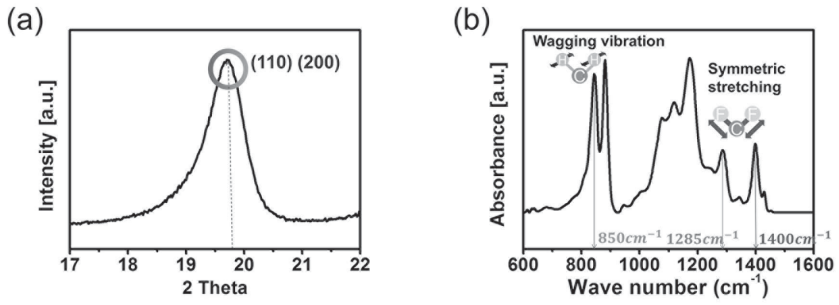

Figure 2. Characterization of β phase of P(VDF-TrFE). a) XRD and b) FT-IR spectroscopy results of the P(VDF-TrFE) thin film.

P(VDF-TrFE) thin film-based PNGs were obtained under the vertical compressive force of 0.15 kgf as shown in **Figure 3**a,b. The output voltage and current of microstructured P(VDF-TrFE)-based PNGs showed high value nearly five times of enhancement was observed in the output voltage and current compared to the flat film-based PNG. The output power variation of the pyramid-shaped micropatterned P(VDF-TrFE)-based PNG was investigated depending upon the loading resistance under the normal compressive force of 0.15 kgf. Figure 3c shows the load resistance dependence of both output voltage and the current with the resistance ranging from 10^4 to 10^9 Ω. The output current decreases as load resistance increases due to the ohmic loss, while the output voltage tends to increase. The maximum power was obtained at a load resistance of 10^6 Ω, corresponding to a peak power of about 2.8 μW (Figure 3d).

To verify that the measured signals were generated by the PNGs device rather than the measurement system, we conducted switching-polarity tests. When the current meter was connected reversely, the pulses were also reversed (see Figure S2, Supporting Information).

The working mechanism of P(VDF-TrFE)-based PNGs can be understood in terms of piezoelectric polarization under mechanical deformation (see Figure S3, Supporting Information). When we applied the electric field poling on the polymers, the electric dipoles into the P(VDF-TrFE) thin film aligned symmetrically (e.g., from top to bottom electrode) due to its ferroelectric property (indicated by arrows). If the P(VDF-TrFE)-based PNGs was subjected to a vertical compressive strain, a positive piezoelectric potential was developed at the bottom side of the P(VDF-TrFE). An opposite negative potential was set up at the top surface of the P(VDF-TrFE). A potential difference was developed between the bottom and top electrodes. As a result, the piezoelectric potential-induced electrons started to flow from the Ag electrode to the ITO electrode through an external load resistor, giving an electric signal under forward connection. As the strain was released, the piezoelectric potential immediately vanished and the electrons accumulated near the ITO electrode flow back through the external circuit to the Ag electrode. An electric signal was observed in opposite direction.

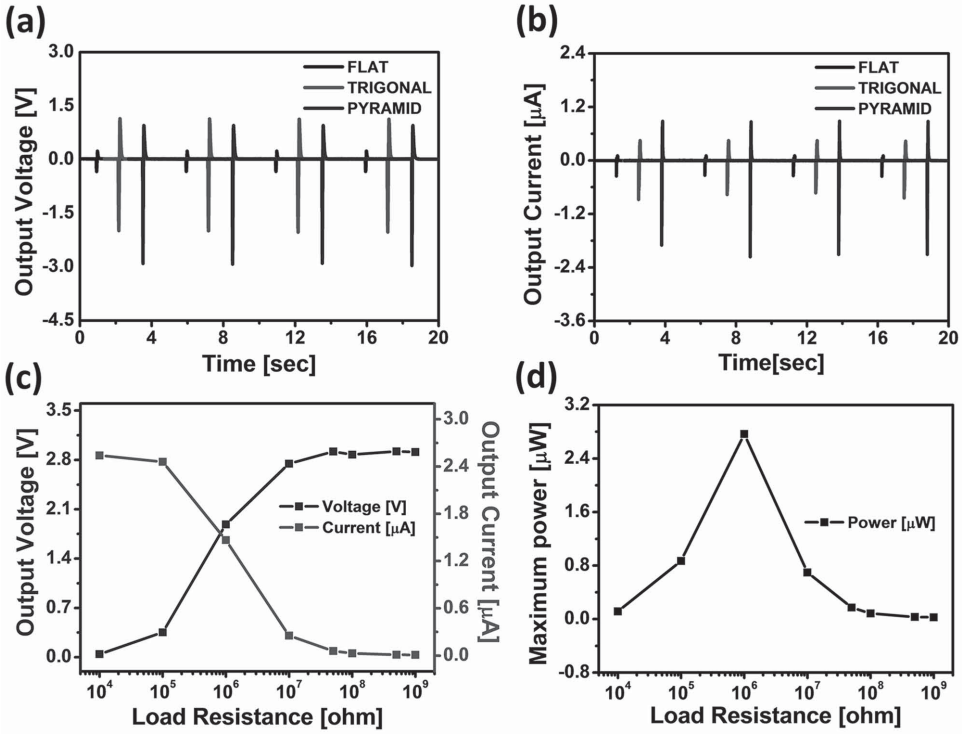

Figure 3. Experimentally observed a) output voltage and b) current from the flat, trigonal line-shaped, and pyramid-shaped P(VDF-TrFE)-based PNGs under the vertically applied constant compressive force of 0.15 kgf. c) Dependence of the output voltage and current as a function of the external load resistance and d) corresponding peak power output at 0.15 kgf.

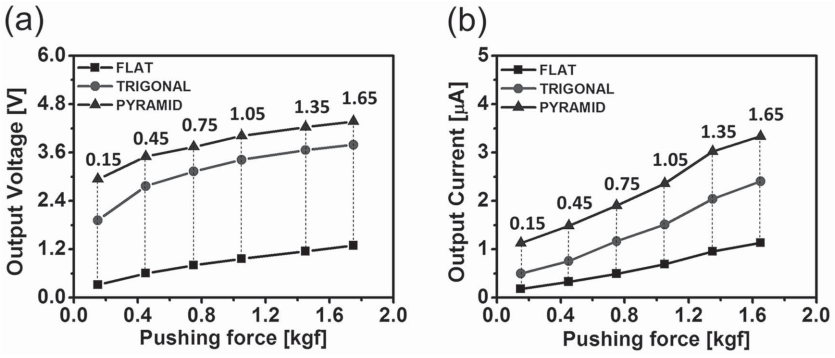

Figure 4. a) Output voltage and b) current from the flat, trigonal line-shaped, and pyramid-shaped P(VDF-TrFE)-based PNGs under various working forces vertically applied onto substrate.

As a result, continuous peak-to-peak electric signal was generated under application of stress and release of force.

The above result demonstrated that the output voltage and current in case of micropatterned P(VDF-TrFE)-based PNGs were significantly larger compared to the flat film-based PNG. This enhancement could be attributed to different strain caused by different degree of sensitivity from the trigonal line-shaped, pyramid-shaped micropatterned as compared to the flat P(VDF-TrFE) film under application of same 1 kgf. It was clear that, although the applied force is same in all cases, due to morphological difference, the strain development was different. The pyramid-shaped micropatterned P(VDF-TrFE)-based PNG exhibited high output performance than that of trigonal line-shaped micropatterned P(VDF-TrFE)-based PNG under same force. To confirm the stability and better performance of pyramid-shaped micropatterned P(VDF-TrFE) over others, the output voltage and current were measured from the flat, trigonal line-shaped, pyramid-shaped P(VDF-TrFE)-based PNGs at different mechanical force.

The magnitude of the output voltage and current generated by the flat, trigonal line-shaped, and pyramid-shaped micropatterned P(VDF-TrFE)-based PNGs under application of force in range from 0.15 to 1.65 kgf are shown in **Figure 4**a,b. It was found that the output voltage and current increased with the increase of force in all NGs. The output voltage and current from pyramid-shaped PNG showed high performance under application of all forces. The output voltage and current reached up to the value of 4.4 V and 3.4 μA from pyramid-shaped P(VDF-TrFE)-based PNG at 1.65 kgf. This results confirmed that pyramid-shaped morphology was the best for high output performance from P(VDF-TrFE)-based PNGs under vertically applied external force. Mechanical durability test results (**Figure 5**a,b) under different pressure of 0.15 and 1.05 kgf confirmed the prominent mechanical durability of the micropatterned P(VDF-TrFE)-based PNGs. A very stable output voltage was obtained over 5000 cycles in all cases (Figure S5, Supporting Information).

To theoretically investigate the difference in the power output from the flat and micropatterned P(VDF-TrFE)-based PNGs, COMSOL simulation investigation was performed. The relation of piezoelectricity can be explained by combination of the electrical behavior of the material (1) and Hooke's Law (2) as given in following equations:

$$D = \varepsilon E \tag{1}$$

$$S = sT \tag{2}$$

where D is the electric charge density displacement, ε is permittivity, E is electric field strength, S is strain, s is compliance, and T is applied stress. To a good approximation, those interaction can be described by linear relations as shown

$$S = s^E T + \mathrm{d}E \tag{3}$$

$$D = \mathrm{d}T + \varepsilon^T E \tag{4}$$

The above equation confirmed that strain variations that gives different piezoelectric output.[30,32] Using the above concept, strain distributions in the flat, trigonal line-shaped, and pyramid-shaped morphology under same constant force were examined. Color-coded results are shown in **Figure 6**. The simulation results depicted that pyramid-shaped structure had strong variation in the stain along the thickness of thin film compared to the flat and trigonal line-shaped micropatterned thin films. Therefore, higher strain produced higher piezoelectric signal, giving higher output voltage and current for the pyramid-shaped microstructured P(VDF-TrFE)-based PNGs.

It was noted that micropatterned P(VDF-TrFE) exhibiting high sensitivity in response of even small force could be utilized as self-powered pressure sensors. One of its practical applications is a mechanical stimuli sensor system. A novel P(VDF-TrFE)-based piezoelectric climate sensing system was developed (**Figure 7**). A virtual sensor module adhered on typical window is recognizable in Figure 7a. Enlarged digital image was provided as an inset. The P(VDF-TrFE)-based pressure detector could alarm a sudden change in weather, such as

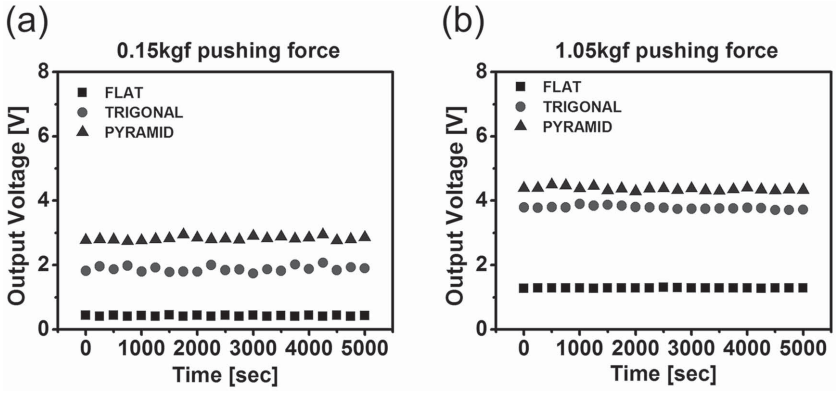

Figure 5. Examination of mechanical durability for different (the flat, trigonal line-shaped, and pyramid-shaped) P(VDF-TrFE) PNGs; a,b) Stable output voltage generation from all P(VDF-TrFE) PNGs with different applied force of 0.15 and 1.05 kgf, respectively.

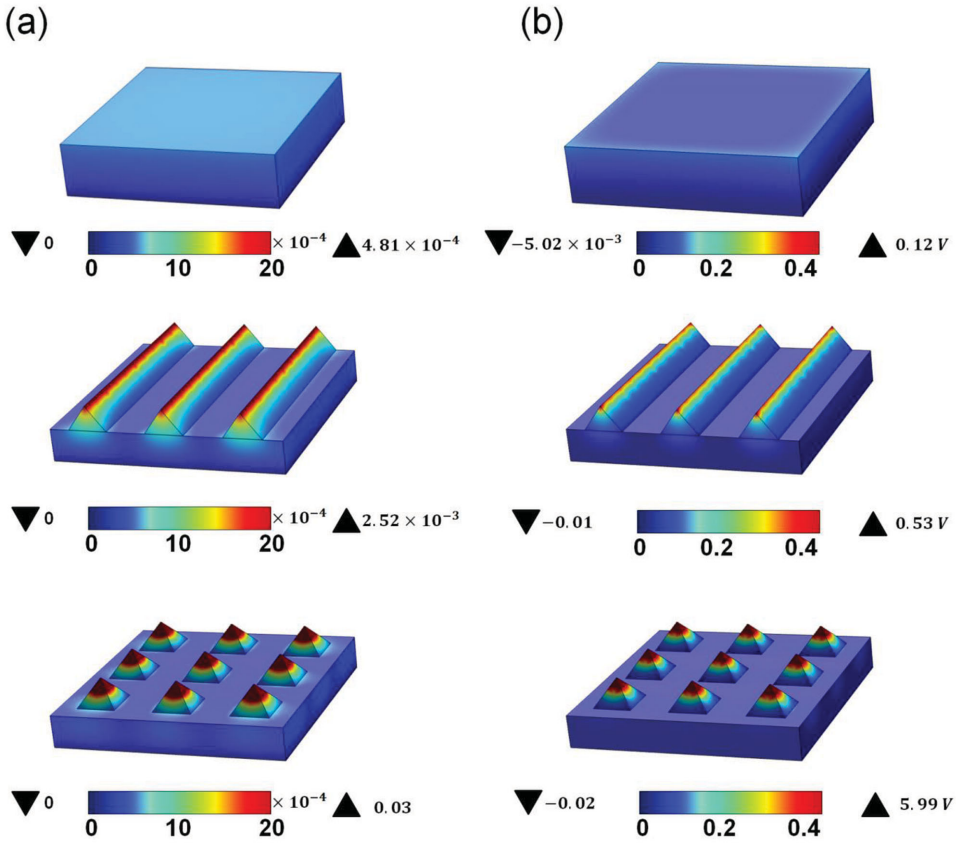

Figure 6. Simulation results showing structured surfaces such as trigonal line-shaped and pyramid-shaped P(VDF-TrFE)-based PNGs. 1 × 1 dimensional devices were modeled employing COMSOL. Total height of all devices was set as 15 μm with applied vertical compression of 0.1 kgf. Derived strain from given stress is shown in a). Further study about output voltage induced by following strain is demonstrated in (b).

raining or wind velocity assumed to be as external force. That is, whatever certain atmospheric changes within the performance induced by devices, it can be operated by itself without any supply of electricity. Maximum transformed output from a given input is the most preferable way. Figure 7b,c shows comparative output voltage data for all types of pressure sensor including the flat, trigonal line-shaped, and pyramid-shaped patterned under raining circumstance and windy case. Detailed experimental set-up for both instances are described in Figure S6 (Supporting Information).

With ≈80 mL of water droplet freely falling 142 mm, enhanced amount of stress was applied on both patterned devices that have an increase in output voltage. The actual water droplet on device is shown as inset. Its diameter was determined through an engineering metal ruler. It was ≈7 mm when it constantly stayed on the device. Another practical application is wind sensor. This innovative system not only enables us to harvest electrical power identical to commercial wind turbines but also provides information of wind strength as a detectable mechanical force. Relatively low speed wind that can deliver small amount of energy to the device can also be recognized as shown in Figure 7c. We found unprecedented sensitivity in an extremely low wind pressure derived from 0.5 m s^{-1} of wind velocity, with patterned surfaces showing

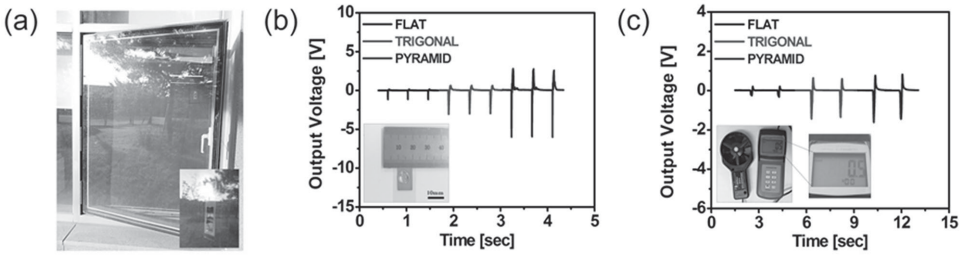

Figure 7. Highly sensitive pressure-sensing devices derived from micropatterned P(VDF-TrFE). a) Climate sensor is situated onto the window outward. Inset: Enlarged illustration of the rain sensor; b) Output voltage generated from all types of sensors with respect to patterns on surface as dropping water droplet. Inset: Water droplets staying at the sensor (scale bar: 10 mm); c) Output voltage induced by sensors regarding the patterns on surface as stirring up the wind using an air gun. Inset: Wind speed was recorded by utilizing an anemometer.

almost five orders of magnitude higher than flat surface. With an air generation system, we could make an artificial windy condition experimentally and measure its speed utilizing commercial anemometer as given in inset of Figure 7c. In all cases, micropatterned surface, especially the pyramid-shaped one, has the highest sensitivity regarding the external pressure, which clearly tells us that structured surface is prominently suitable for detecting minuscule stress. It is quite effective for microstructured surface to be used to respond rapidly to external stimuli. This can be used in alarm system such as for rain starting or wind rising without any electrical energy storage such as battery.

3. Conclusion

In summary, we successfully enhanced the electric output power from P(VDF-TrFE)-based PNGs via a simple micropattering process. Two different types of morphologies (trigonal line-shaped and pyramid-shaped) were developed on P(VDF-TrFE) polymer using photolithography and their PNGs were fabricated. The output voltage and current were measured from the flat and micropatterned piezoelectric P(VDF-TrFE) polymers under vertical compressive force. Higher output voltage and current with average values of 4.4 V and 3.4 μA were obtained from the micropatterned P(VDF-TrFE)-based PNG under vertical mechanical compressive force compared to the flat film-based PNG (1 V and 100 nA). The pyramid-shaped micropatterned P(VDF-TrFE)-based PNG exhibited larger power output than the trigonal line-shaped micropatterned P(VDF-TrFE)-based PNG. The output performance was increased with the increase of compressive force. Very stable electric power generation performance over 5000 cycles was obtained. The enhancement in the output power was discussed using COMSOL simulation in term of different strain created in the flat and micropatterned piezoelectric film under the same constant force. Due to its ultrahigh sensitivity, the micropatterned PNGs were also demonstrated as a self-powered pressure sensor. Our demonstration of power enhancement in micropatterned P(VDF-TrFE)-based PNGs may greatly contribute to the development of self- powering small scale devices or systems with low operating power consumption.

4. Experimental Section

Synthesis of Micropatterned P(VDF-TrFE) and Fabrication of PNGs: P(VDF-TrFE) solution was prepared by dissolving P(VDF-TrFE) copolymer powder in *N*,*N*-dimethylformamide (DMF) with stirring for 12 h at room temperature. Solution of P(VDF-TrFE) (≈20 wt%) was spin-coated on flexible ITO-coated PEN substrate at 3000 rpm for 60 s, followed by drying at 80 °C to remove the DMF solvent. For micropattering, trigonal line-shaped, and pyramid-shaped patterned Si wafer master mold was fabricated from (100) Si wafers with a 300 nm thermally grown oxide by simple photolithography and etching process to release the mold. Micropatterned layer was annealed at 140 °C for 2 h and then naturally cooled down to room temperature gradually in order to enhance the crystallinity of the β phase. For device fabrication, Ag electrode of average thickness of 200 nm was deposited by using a thermal evaporation method. The electrical poling process was carried out by applying an external electric field of 80 MV m^{-1} for 2 h to align the electric dipoles in a single direction.

Characterization and Measurements: FE–SEM characterization was performed for the morphological investigation of the flat, trigonal line-shaped, and pyramid-shaped micropatterned P(VDF-TrFE) films. The synthesized piezoelectric polymers underwent structural and crystallographic characterizations using XRD (Bruker D8 DISCOVER) with Cu KR radiation (λ = 1.54 Å). FT-IR measurements were used for the structural investigation of the β phase of P(VDF-TrFE) thin films. A pushing tester (Labworks Inc., Model No. ET-126-4) was utilized to create strain in P(VDF-TrFE). A Tektronix DPO 3052 Digital Phosphor Oscilloscope and low-noise current preamplifier (Model No. SR570, Stanford Research Systems, Inc.) were used to measure electrical signal.

Supporting Information

Supporting Information is available from the Wiley Online Library or from the author.

Acknowledgements

J.-H.L. and H.-J.Y. contributed equally to this work. This work was financially supported by Basic Science Research Program (2012R1A2A1A01002787, 2009-0083540) and the Center for Advanced Soft-Electronics as Global Frontier Project (2013M3A6A5073177) through the National Research Foundation (NRF) of Korea Grant funded by the Ministry of Science, ICT and Future Planning.

Received: March 3, 2015
Revised: March 20, 2015
Published online: April 15, 2015

[1] Z. L. Wang, J. Song, *Science* **2006**, *312*, 242.
[2] S. Xu, Y. Qin, C. Xu, Y. Wei, R. Yang, Z. L. Wang, *Nat. Nanotechnol.* **2010**, *5*, 366.
[3] Z. L. Wang, *Adv. Mater.* **2011**, *24*, 279.
[4] S. Wang, L. Lin, Z. L. Wang, *Nano Lett.* **2012**, *12*, 6339.
[5] Y. Qin, X. Wang, Z. L. Wang, *Nature* **2008**, *451*, 809.
[6] X. Wang, J. Song, J. Liu, Z. L. Wang, *Science* **2007**, *316*, 102.
[7] J.-H. Lee, K. Y. Lee, B. Kumar, N. T. Tien, N.-E. Lee, S.-W. Kim, *Energy Environ. Sci.* **2013**, *6*, 169.
[8] S. N. Cha, J.-S. Seo, S. M. Kim, H. J. Kim, Y. J. Park, S.-W. Kim, J. M. Kim, *Adv. Mater.* **2010**, *22*, 4726.
[9] S. Bai, Q. Xu, L. Gu, F. Ma, Y. Qin, Z. L. Wang, *Nano Energy* **2012**, *1*, 789.
[10] Y. Hu, Y. Zhang, C. Xu, L. Lin, R. L. Snyder, Z. L. Wang, *Nano Lett.* **2011**, *11*, 2572.
[11] W. Wu, S. Bai, M. Yuan, Y. Qin, Z. L. Wang, T. Jing, *ACS Nano* **2012**, *6*, 6231.
[12] S. Lee, S.-H. Bae, L. Lin, Y. Yang, C. Park, S.-W. Kim, S. N. Cha, H. Kim, Y. J. Park, Z. L. Wang, *Adv. Funct. Mater.* **2013**, *23*, 2445.
[13] Y. Yang, H. Zhang, Z. H. Lin, Y. S. Zhou, Q. Jing, Y. Su, J. Yang, J. Chen, C. Hu, Z. L. Wang, *ACS Nano* **2013**, *7*, 9213.
[14] G. Zhu, R. Yang, S. Wang, Z. L. Wang, *Nano Lett.* **2010**, *10*, 3151.
[15] B. Kumar, S.-W. Kim, *Nano Energy* **2012**, *1*, 342.
[16] J. H. Song, J. Zhou, Z. L. Wang, *Nano Lett.* **2006**, *6*, 1656.
[17] S. Xu, B. J. Hansen, Z. L. Wang, *Nat. Commun.* **2010**, *1*, 93.
[18] J. Jung, M. Lee, J.-I Hong, Y. Ding, C.-Y. Chen, L.-J. Chou, Z. L. Wang, *ACS Nano* **2011**, *5*, 10041.

[19] Y. Yang, J. H. Jung, B. K. Yun, F. Zhang, K. C. Pradel, W. Guo, Z. L. Wang, *Adv. Mater.* **2012**, *24*, 5357.
[20] K.-I. Park, S. Xu, Y. Liu, G.-T. Hwang, S.-J. L. Kang, Z. L. Wang, K. J. Lee, *Nano Lett.* **2010**, *10*, 4939.
[21] K. Y. Lee, D. Kim, J.-H. Lee, T. Y. Kim, M. K. Gupta, S.-W. Kim, *Adv. Funct. Mater.* **2014**, *24*, 37.
[22] K. Omote, H. Ohigashi, K. Koga, *J. Appl. Phys.* **1997**, *81*, 2760.
[23] H. Xu, Z.-Y. Cheng, D. Olson, T. Mai, Q. M. Zhang, *Appl. Phys. Lett.* **2001**, *78*, 2360.
[24] S. N. Cha, S. M. Kim, H. J. Kim, J. Y. Ku, S. I. Sohn, Y. J. Park, B. G. Song, M. H. Jung, E. K. Lee, B. L. Choi, J. J. Park, Z. L. Wang, J. M. Kim, K. Kim, *Nano Lett.* **2011**, *11*, 5142.
[25] X. Wang, *Nano Energy* **2012**, *1*, 13.
[26] J. Chang, M. Dommer, C. Chnag, L. Lin, *Nano Energy* **2012**, *1*, 356.
[27] J.-H. Lee, K. Y. Lee, M. K. Gupta, T. Y. Kim, D.-Y. Lee, J. Oh, C. Ryu, W. J. Yoo, C.-Y. Kang, S.-J. Yoon, J.-B. Yoo, S.-W. Kim, *Adv. Mater.* **2014**, *26*, 765.
[28] Z. Pi, J. Zhang, C. Wen, Z.-B. Zhang, D. Wu, *Nano Energy* **2014**, *7*, 33.
[29] E. S. Nour, M. O. Sandberg, M. Willander, O. Nur, *Nano Energy* **2014**, *9*, 221.
[30] W. Zeng, X.-M. Tao, S. Chen, S. Shang, H. L. W. Chan, S. H. Choy, *Energy Environ. Sci.* **2013**, *6*, 2631.
[31] Z. H. Liu, C. T. Pan, L. W. Lin, H. W. Lai, *Sens. Actuators A* **2013**, *193*, 13.
[32] V. V. Kochervinskii, *Crystallogr. Rep.* **2003**, *48*, 649.